THE JOURNAL OF PHYSICAL CHEMISTRY C

Article

pubs.acs.org/JPCC

Dopants in Lanthanum Manganite: Insights from First-Principles Chemical Space Exploration

Sridevi Krishnan,*[,†,‡] Vinit Sharma,[†,‡,¶] Prabhakar Singh,[†,§] and Rampi Ramprasad*[,†,‡]

[†]Materials Science and Engineering, University of Connecticut, Storrs, Connecticut 06269, United States

[‡]Institute of Materials Science, University of Connecticut, Storrs, Connecticut 06269, United States

[§]Center for Clean Energy Engineering, University of Connecticut, Storrs, Connecticut 06269, United States

Supporting Information

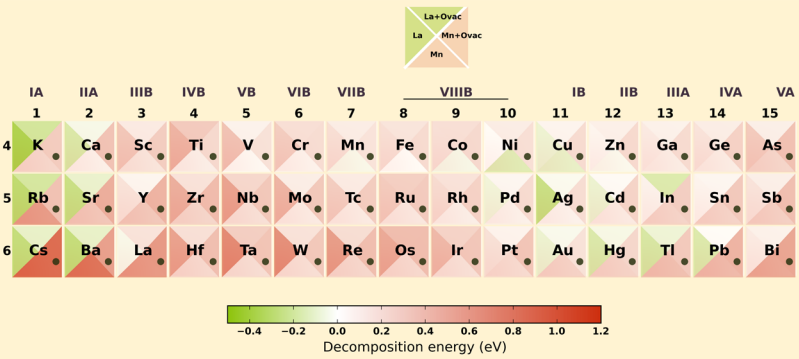

ABSTRACT: The dopant chemical space in $LaMnO_3$ (LMO) is systematically explored using first-principles computations. We study a range of cationic dopants including alkali, alkaline earth metals, 3d, 4d, and 5d transition metal elements without and with an adjacent O vacancy. A linear programming approach is employed to access the energetically favorable decomposition pathway and the corresponding decomposition energy of doped $LaMnO_3$. The decomposition energy is then used to classify the dopants for stability, site preference and tendency of O vacancy formation. We find that La site doping is more favored compared to Mn site doping. We also identify dopants previously not considered, such as K, Rb, Cs, and In, which lead to stable doped LMO and are also excellent O vacancy formers. Employing data mining techniques, we identify the dopant features that are critical to the stability of a doped oxide.

INTRODUCTION

Oxide perovskites are an attractive class of materials with a broad array of technological applications,[1,2] owing to their exceptional physical and chemical properties. The remarkable ability of the perovskite structure with the generic formula ABO_3 to host a variety of A and B site cationic elements leads to different materials with a host of interesting properties. In addition, doping in either of the cationic sites opens up avenues for further tailoring the material properties. Doped lanthanum Manganite ($LaMnO_3$ or LMO) is one such oxide perovskite with an array of applications[3−5] including in solid oxide fuel cells,[6,7] giant magneto resistance devices,[8] and catalytic combustion.[9] Although a few dopants in LMO have been explored,[10−16] a comprehensive study of the many possible dopants at a consistent level of theory is unavailable at this time. Such a study will provide very useful insights pertaining to the stability of a dopant in LMO or similar oxide.

In recent years, the community has resorted to large scale chemical space searches (via high-throughput computing) in which several possible candidates are initially considered in an unbiased and uniform manner.[17−29] Such a strategy is particularly useful either when chemical intuition concerning the relevant cases are unavailable (thereby preventing further significant progress), or when predictive models based on quantitative trends and correlations across a chemical series is desired. Indeed, these strategies have led to several successful discoveries of new materials.[30−37]

Here, we employ a systematic search of the dopant chemical space to identify stable and desirable dopants in LMO. To aid this search, we explore cationic dopants ranging from the alkali and alkaline earth metals, 3d, 4d, and 5d series transition metals through group VA of the periodic table (K−As, Rb−Sb, and Cs−Bi) amounting to a total of 44 dopants. In order to probe the role of the dopant on O chemistry, all doped cases were considered without and with an O vacancy adjacent to the dopant atom.

A linear programming approach was used to determine the energetically most favorable decomposition pathway (or products) if any, for each case, and the corresponding decomposition energy. The dopants were then assessed based

Received: May 4, 2016
Revised: July 18, 2016
Published: July 26, 2016

DOI: 10.1021/acs.jpcc.6b04524
J. Phys. Chem. C 2016, 120, 22126−22133

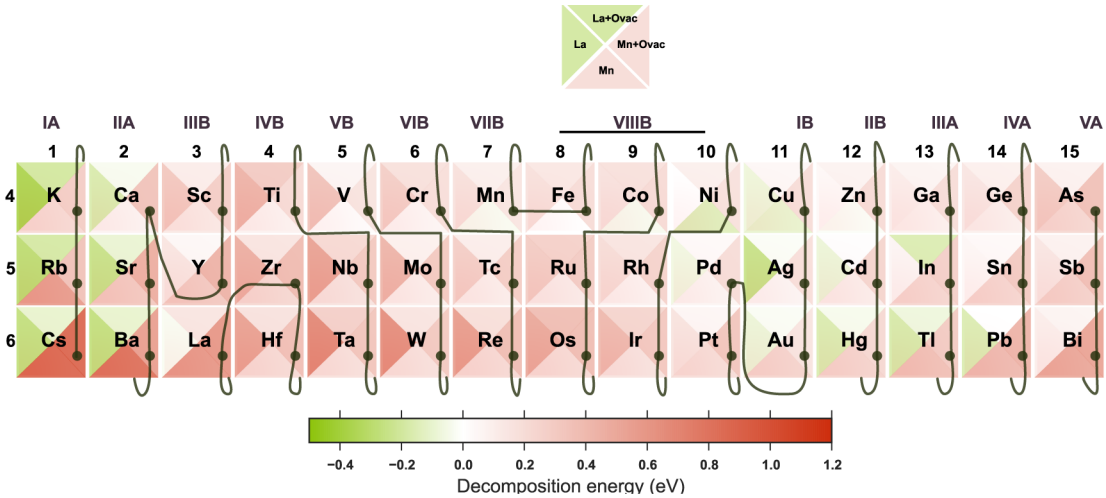

Figure 1. Dopants from the periodic table considered in this study. The decomposition energy (E_d^D) of the compound with a substitutional dopant in the La and Mn site both without and with an adjacent O vacancy in the vicinity of the dopants is represented by the left, bottom, top and right triangles, respectively. The decomposition energy is color coded and the color bars shows the scale for the decomposition energy. The doped compound is considered stable against decomposition when $E_d^D < 0$ eV. The gray line connecting the dots represents the string for Mendeleev number ordering.

on the resistance of the doped oxide to decomposition, the tendency of O vacancy formation and the site preference based on the decomposition energy.

Our strategy correctly recovers dopants already known to be efficacious for enhancing O vacancy formation in LMO. Additionally, we identify new dopants, including K, Rb, Cs and In, which are expected to lead to stable doped LMO that are simultaneously superior O vacancy formers. This trend is visually captured in Figure 1, which displays the stability of doped LMO with the dopant in the A or B site and without or with an adjacent O vacancy (green shades indicate cases and situations with high stability). Data mining methods[38] were employed to identify trends and correlations between the dopant properties and the stability of the compounds. It is hoped that this work will spur future experimental studies of these doped oxides.

METHODS

Models. The room temperature structure of LMO is orthorhombic;[39] however, applications involving high temperature operations like SOFC, the structure becomes cubic. Therefore, we chose the cubic perovskite structure for all our calculations. We then substitutionally doped the cations K−As, Rb−Sb, and Cs−Bi at the La or Mn sites in a 2 × 2 × 2 supercell, resulting in a dopant concentration of 12.5%. In addition, a neutral O vacancy in the vicinity of each dopant was considered. Altogether, four different sets of calculations with dopants (D) in the La ($La_{1-a}D_aMnO_{3-\delta}$) and Mn ($LaMn_{1-a}D_aO_{3-\delta}$) sites without ($\delta = 0$) and with ($\delta = 0.125$) an O vacancy were performed. For consistency, all of the compounds were initialized in a ferromagnetic (FM) state and allowed to relax to their ground state.

Computational Details. Spin polarized calculations were performed using density functional theory as implemented in the VASP[40,41] code. The electron exchange-correlation interaction was treated using the generalized gradient approximation (GGA) with Perdew−Burke−Ernzerhof (PBE)[42] functional. The projector augmented wave (PAW) potentials[43] were used to describe the core states. All calculations were performed with a cutoff energy of 520 eV and a 4 × 4 × 4 Monkhorst−Pack *k*-point grid was used to sample the brillouin zone. The atomic positions were relaxed in the cubic supercell until the force on each atom fell below a threshold of 0.02 eV/Å.

Stability. Conventionally, the thermodynamic stability of a doped compound is estimated from the calculated formation energy. The formation energy can be defined in multiple ways depending on the reference chosen for elemental chemical potentials.

However, what is more relevant to stability is the tendency of a compound, once formed, to resist decomposition. The decomposition energy of a compound such as doped LMO is far more difficult to compute than an appropriately defined formation energy, as there can be a plethora of decomposition products, including some combination of the relevant metallic elements/alloys, binary oxides and ternary oxides.

In order to find the most expected decomposition pathway, all the possible combinations of the decomposition reactions should be studied and their corresponding energies compared. Alternatively, a constrained optimization can find the most thermodynamically favored set of products subject to stoichiometry preserving constraints (as described below).

The linear programming (LP) method[44−48] offers an efficient approach to find the most expected set and amounts of products for the doped compounds. This involves listing the possible product compounds (the "product pool"), which in our case included the elemental metals, their binary oxides, LMO and oxygen molecule. The coefficients c_i corresponding to each of these product compounds represent the amount of each product compound contained in the final set of products. The decomposition energy of a doped LMO with dopant D, E_d^D, is then defined as

$$E_d^D = E_{LMO}^D - \min_{c_i} \begin{cases} c_1E_{La(s)} + c_2E_{Mn(s)} + c_3E_{D(s)} \\ + c_4E_{La_2O_3(s)} + c_5E_{Mn_2O_3(s)} \\ + c_6E_{D_yO_x(s)} \\ + c_7E_{LaMnO_3} + c_8E_{O_2} \end{cases} \quad (1)$$

DOI: 10.1021/acs.jpcc.6b04524
J. Phys. Chem. C 2016, 120, 22126−22133

where E^D_{LMO} is the DFT energy of the doped compounds (with the dopant at the La or the Mn site, and with or without an adjacent O vacancy) and all the Es in the second term are DFT energies of all possible elemental, binary and ternary oxides considered as products.

The c_i coefficients that minimize the second term of eq 1 are determined subject to the following stoichiometry preservation constraints:

$$c_1 + 2c_4 + c_7 = 1 - a$$
$$c_2 + 2c_5 + c_7 = 1$$
$$c_3 + yc_6 = a$$
$$3c_4 + 3c_5 + xc_6 + 3c_7 + 2c_8 = 3 - \delta \quad (2)$$

$$c_i \geq 0 \quad (3)$$

To understand the above constraints, let us consider an example. The stoichiometry of La in $La_{1-a}D_aMnO_{3-\delta}$ is $1 - a$; thus, the sum of all c_is of compounds involving La (namely c_1, c_4, and c_7) should be equal to $1 - a$, leading to the first equality of eq 2. The minimization of the second term in the right-hand side of eq 1 subject to the constraints in eq 2 and 3 will lead to the most expected products. For each choice of dopant D, 4 decomposition energies (corresponding to the dopant at the La or the Mn site, and in each case with or without an adjacent O vacancy) were computed. The energies and structures of all elemental metals and binary oxides (all in their most favored standard states) are contained in the Supporting Information and are also available at the online repository (see Figure S1).[49]

As mentioned above, the formation energies of these compounds can be calculated for different choices of the elemental chemical potential references. We have calculated the formation energy based on two such references and the correlation of these energies with that of decomposition energy is also discussed in the Supporting Information.

Factors Affecting the Accuracy of Energies. It is well-known that GGA over binds the oxygen molecule.[27] To correct for this overbinding a shift of 1.38 eV/O_2 molecule is used to destabilize the total energy of the O_2 molecule, consistent with similar procedures adopted in the past.[27,50,51]

The conventional DFT treatment based on semilocal exchange-correlation potentials is known to be insufficient in highly correlated materials.[52] Higher order methods like DFT +U and hybrid methods could be employed to address this concern. However, the determination of the U parameter in the DFT+U method for each of the dopants included here is a formidable task. Besides, the transferability of the U parameters between different chemical environments is questionable.[53] Similarly, the computational cost involved in employing hybrid or other advanced exchange-correlation functionals is also challenging considering the number of dopants studied here. Therefore, we proceed with the GGA-PBE level of theory and aim to give a consistent comparative description (across the large chemical series considered) of the effect of the dopant and defects in LMO. Nevertheless, in order to obtain an idea of the sort of deviations one may obtain in the results if a higher level theory was used, we adopted PBE+U calculations for a dozen La-site dopant cases (with the U-J value for Mn taken to be 4 eV, following previous work[12]). We found that the PBE and PBE+U results follow the same trends, with the standard deviation in the decomposition energy between the two treatments being 0.06 eV. We thus believe that the overall trends across the chemical series as determined by the PBE functional is reliable.

Two other factors that have not been considered here are the entropic contributions to the energies, and non-neutral charged states of O vacancies. While these factors indeed may be important, we expect that their impact on the general trends we obtain here will be minimal (insofar as the relative tendencies for decomposition and O vacancy formation are concerned). Moreover, given the vast dopant chemical space examined here, consideration of all possible factors for every case is hardly practical. Thus, our view is that such more detailed and in-depth studies of promising specific cases can be taken up in future studies.

RESULTS AND DISCUSSIONS

Stability of Doped LMO. The decomposition energy, E^D_d, as defined in eq 1 may be used to draw several important and useful conclusions, including those related to (1) whether a doped LMO, once created, will remain stable, (2) whether a dopant prefers to be in the La or the Mn site, and (3) whether a dopant will lead to the formation of O vacancies. Below, we address each of these points in a systematic manner.

The doped compound is considered stable if $E^D_d < 0$ eV, with more negative values representing situations with higher levels of stability. Figure 1 captures the trend displayed by the decomposition energy across the range of dopants considered in a visually obvious manner. For each choice of dopant, four different E^D_d values are reported corresponding to (1) the dopant in the La site (left quarter), (2) the dopant in the La site with an adjacent O vacancy (top quarter), (3) the dopant in the Mn site (bottom quarter), and (4) the dopant in the Mn site with an adjacent O vacancy (right quarter). Each quarter is color-coded so that positive and negative values of E^D_d are represented using red and green gradients, respectively, and whiter shades represents E^D_d values close to zero.

From Figure 1, it is immediately evident which doped oxides can be expected to be stable. Of the 44 dopants considered (i.e., the 45 elements shown in Figure 1 minus the host element, be it La or Mn), only a handful lead to stable doped oxides. These are the ones represented using greenish shades in at least one of the quarters in a given square. Focusing, for the moment, on just the left and bottom quarters, we note that the dopants that lead to stable doped LMO compounds include K, Rb, Cs, Ca, Sr, Ba, Pd, Cu, Ag, Au, Cd, Hg, Tl, and Pb (in the La site) and Co, Ni, Cu, and Zn (in the Mn site). Among these, the most stable ones (i.e., those that display the darkest green quarters) are those involving the alkali and alkaline earth elements (i.e., K, Rb, Cs, Ca, Sr, Ba). Indeed, all these findings are entirely consistent with available experimental evidence for both La[54−59] and Mn[4,60] site doping. We note though that K, Rb and Cs have not been considered in experimental work in the past, and hence, constitute new dopants identified by this study. Our results are also collected in Table. 1.

A corollary to the above finding is the recognition of the site preference of the dopants. From the above list, and from a visual inspection of Figure 1, it is evident that La site doping is far more favorable than Mn site doping, again, a notion consistent with experience and experiments. Even those dopants that do show a tendency to occupy the Mn site (which include Co, Ni, Cu, and Zn) lead only to a marginal level of stability of the doped compound.

Next, we comment about the tendency for a doped oxide to support O vacancies, a point captured by the top and right

DOI: 10.1021/acs.jpcc.6b04524
J. Phys. Chem. C 2016, 120, 22126−22133

Table 1. Summary of all Dopants with Decomposition Energy (E_d^D) < 0, when Doped in the La or Mn site without and with an Adjacent O Vacancy[a]

dopants leading to stable oxides	La-site	K, Rb, Cs, Ca, Sr, Ba, Pd, Cu, Ag, Au, Cd, Hg, Tl, Pb
	Mn-site	Co, Ni, Cu, Zn
O vac formers	La-site	K, Rb, Cs, Ca, Sr, Ba, Ag, Au, Hg, Tl, In

[a]The table complements the Figure 1 and gathers all promising dopants identified by this study.

quarters in the squares of Figure 1. Those dopants that lead to greenish colors in these quarters are K, Rb, Cs, Ca, Sr, Ba, Ag, Au, Hg, Tl, and In, all in the La site; these are also listed in Table. 1. Interestingly, barring In, this is a subset of the La site dopants encountered above. Not a single dopant in the Mn site leads to an enhanced tendency for O vacancy formation. This is not surprising as Mn site dopants, even without an O vacancy, lead to only marginally stable doped compounds. It is worth noting that the alkaline earth metal dopants in the La site are already known to be good O vacancy promoters and are being widely studied for SOFC applications.[13] An important outcome of this study is the identification of In as a potential dopant that can encourage the formation of O vacancies. This, like the K, Rb, and Cs cases mentioned above, have not been considered previously in experimental studies.

In order to allow for a quantitative assessment of the decomposition energy, we also plot E_d^D for all the cases considered in Figure 2, in which the dopants are ordered as per their Mendeleev number. This ordering is also shown using a string connecting dots in Figure 1. It can be seen from Figure 2 that dopant elements with similar Mendeleev numbers lead to similar E_d^D values (note, for instance, the alkali and alkaline earth element cluster in the far left of Figure 2).

Finally, we comment about the likely decomposition products in the case of doped LMO that are prone to decomposition. Figure 3 portrays, using a bubble chart, the amount of each of the compounds from the product pool that will result if a doped LMO compound decomposes. Those cases that are deemed stable have a bubble in the topmost row of each panel (corresponding to the doped oxide). The size of the bubble represents the amount of that particular product; we note that pure LMO, by itself, does not display a tendency to decompose to its simple oxides, La_2O_3 and Mn_2O_3, and is hence stable against decomposition. While no generalization can be made, it appears that those cases that are unstable decompose to pure LMO, La_2O_3, and some combination of Mn, D, and their oxides. Pure La is predominantly absent as a decomposition product.

Data Mining. Data mining techniques provide powerful ways to identify useful patterns and trends.[38] Here we employ such statistical (or machine) learning methods to identify significant features that control the stability of a doped LMO oxide.

Kernel ridge regression (KRR),[38,61−64] a nonlinear and regularized regression method was used as the learning model here. KRR maps the input features to a higher dimensional space so that a linear relation may be attained between the features (e.g., properties of dopants) and the associated properties (e.g., the decomposition energy of the doped oxide). It uses the "distances" (or differences) between the features rather than the features themselves and can be regarded as a similarity-based method. This method has been successful in many material property prediction efforts[65−68] and is used here to systematically find the combination of features that lead to the best predictive models.

The target property here was E_d^D and features included the relative deviation of properties of the dopants from that of the host atom, including the oxidation state, Shannon's ionic radius,[69] Pauling electronegativity, ionization energy, and electron affinity. All possible combinations of the 5 features were used in the model to learn from the training data. In each case, 90% of the data set was classified as the training set while the rest as the test set. The root-mean-square error (RMSE) for the test set was then plotted against the number of features for the La and Mn site dopants. The combination of features leading to the least test error was then identified.

For the La-site dopants, a combination of four features including the oxidation state mismatch (OSM), ionic radii mismatch (IRM), ionization energy mismatch (IEM) and electronegativity mismatch (ENM) leads to the minimum test error of 0.070 eV (Figure 4a). However, for the Mn-site dopants (Figure 4b), the test error is an order of magnitude higher than that for the La site dopants. It is clear that the larger radii Cs and Ba cations in the Mn site leads to higher E_d^D and these outliers increase the test error (blue stars in Figure 4b). Removing these outliers from the data set leads to significantly reduced test error (blue triangles in Figure 4b). After excluding the outliers, a features set including just IRM, OSM and IEM

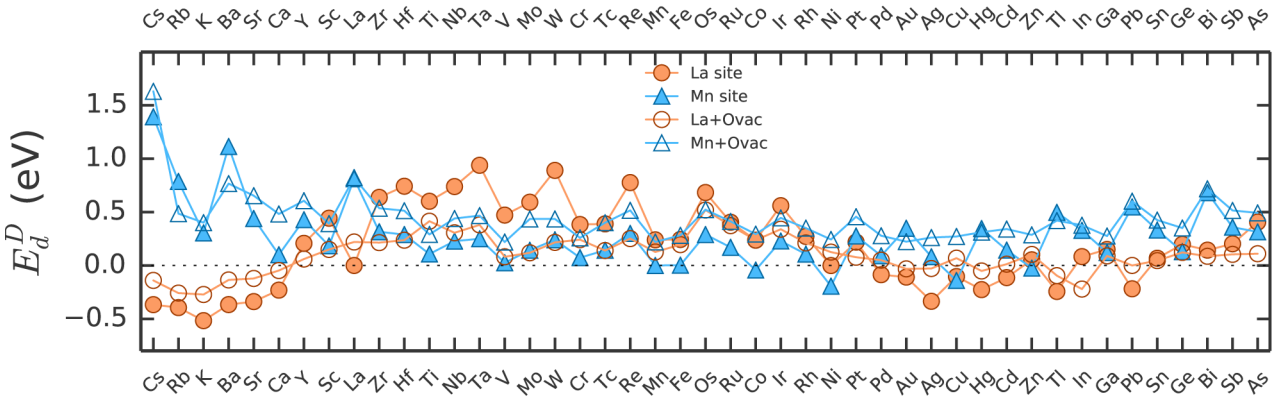

Figure 2. Decomposition energy (E_d^D) for all the dopants considered in the study without and with an O vacancy. The elements in the *x*-axis are arranged in the order of increasing Mendeleev number. The dashed horizontal line corresponds to $E_d^D = 0$.

DOI: 10.1021/acs.jpcc.6b04524
J. Phys. Chem. C 2016, 120, 22126−22133

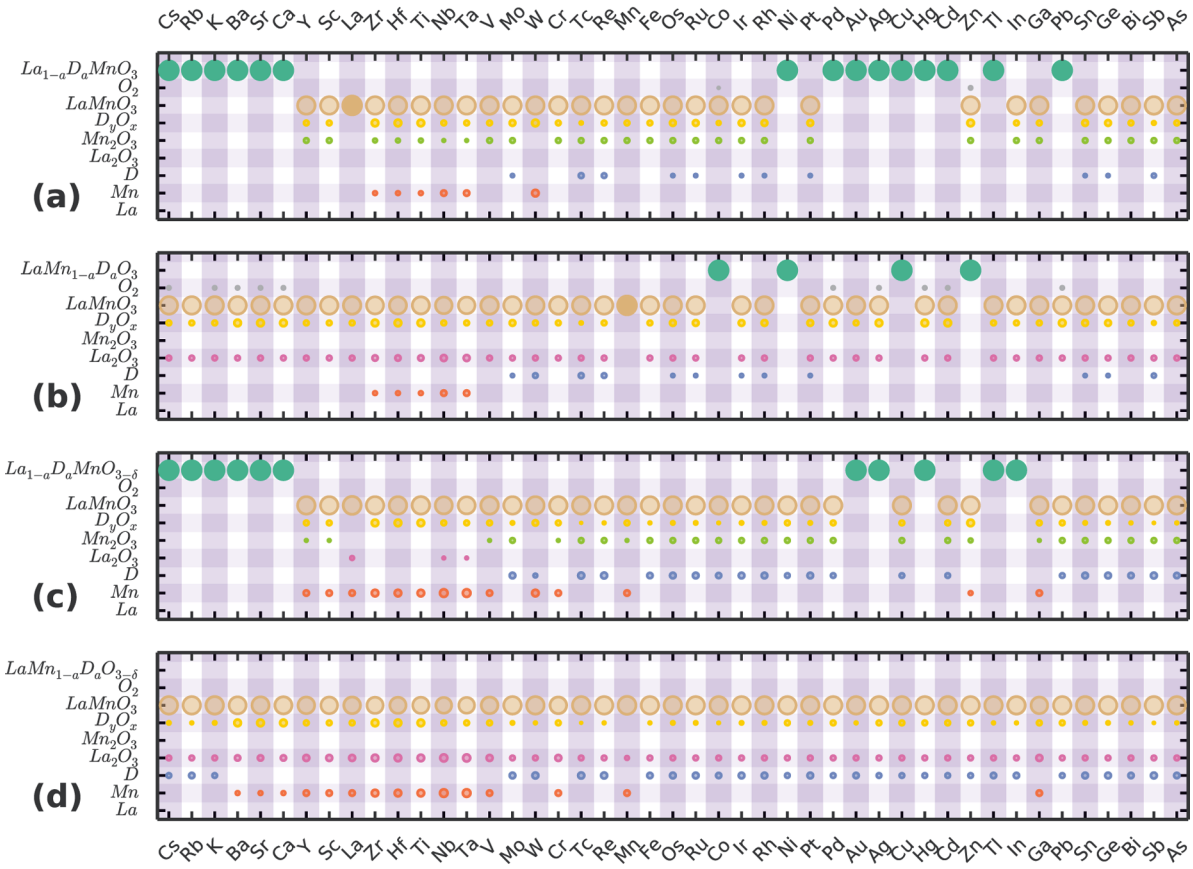

Figure 3. Bubble chart showing the c_i coefficients of eq 1. The rows correspond to the parent doped compound and the eight reaction products considered, and the columns represent the dopants. The bubble sizes are proportional to the c_i values. The panels are for (a) the dopant in the La site, (b) the dopant in the Mn site, (c) the dopant in the La site with an adjacent O vacancy, and (d) the dopant in the Mn site with an adjacent O vacancy.

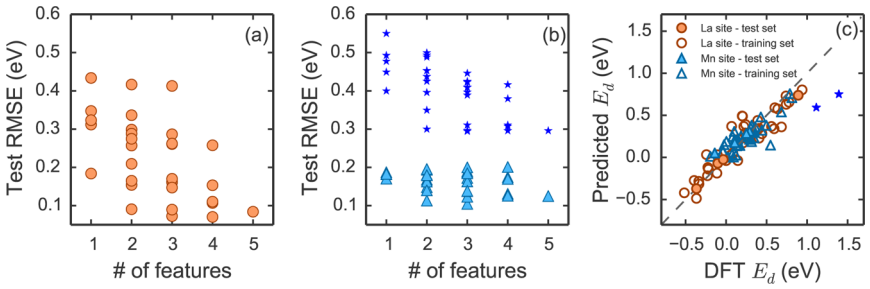

Figure 4. Ranking of features using kernel ridge regression (KRR). The root-mean-square error (RMSE) of the test set is plotted for all possible combination of the five features (oxidation state, Shannon's ionic radius, Pauling electronegativity, ionization energy, and electron affinity mismatch) in the La and Mn site dopants (a and b). The stars and triangles in part b represent the Mn site dopants including and excluding the outliers respectively in the data set. Panel c shows the parity plot of the KRR predicted decomposition energy using the best features vs the DFT calculated decomposition energy. The outliers in the Mn site dopants are excluded in the KRR prediction, but shown as blue stars for comparison.

leads to the minimum test error of 0.105 eV. Subsequently, the feature sets with minimum test error for each case were used to perform E_d^D predictions on the entire data set. The parity plot in Figure 4c compares the KRR predicted and DFT calculated E_d^D values. The analysis reveals that a prediction model of the decomposition energies of the doped oxides may indeed be developed based on key dopant attributes.

■ CONCLUSION

A systematic exploration of a range of substitutional dopants in $LaMnO_3$ at either the La or the Mn site, without and with an adjacent O vacancy was performed using DFT computations. The energetically favorable decomposition pathways and the corresponding decomposition energies of the doped oxides were computed. The decomposition energy was then used to evaluate the stability of the doped compounds, the dopant site preference, and the tendency of O vacancy formation in the doped compounds. Our findings are summarized below:

- The cationic dopants that lead to the most stable doped compounds in the La site are the alkali and alkaline earth elements. For the Mn site, only the transition metal elements Co, Ni, Cu, and Zn lead to a stable doped compound.

DOI: 10.1021/acs.jpcc.6b04524
J. Phys. Chem. C 2016, 120, 22126−22133

- Doping in the La site is more favorable compared to Mn site doping in general.
- The alkali and alkaline earth metals, and the element In in the La site are strong O vacancy promoters whereas none of the Mn site dopants favor O vacancy formation in the doped compound.
- While a general, thermodynamically favorable decomposition pathway is not revealed, most of the unstable doped compounds decompose in to pure LMO, La_2O_3, and some combination of Mn, dopant, and their oxides.
- A data-driven predictive model based just on the ionic radius, oxidation state, electronegativity and the ionization energy mismatch between the host and dopant is shown to be sufficient to predict the decomposition energy of the doped LMO compounds.

Our approach correctly predicts the dopants already known to be effective O vacancy formers in LMO. We also identify dopants previously not considered, such as K, Rb, Cs, and In, which lead to stable doped LMO and are also excellent O vacancy formers.

■ ASSOCIATED CONTENT

Supporting Information

. The Supporting Information is available free of charge on the ACS Publications website at DOI: 10.1021/acs.jpcc.6b04524.

Additional information on the binary oxides used, the conventional formation energy of the doped compounds, and data mining methods for feature ranking[49] (PDF)

■ AUTHOR INFORMATION

Corresponding Authors

*(S.K.) E-mail: sridevi.krishnan@uconn.edu.
*(R.R.) E-mail: rampi.ramprasad@uconn.edu.

Present Address

¶Materials Science and Technology Division, Oak Ridge National Laboratory, Oak Ridge, TN 37831

Notes

The authors declare no competing financial interest.

■ ACKNOWLEDGMENTS

This work is supported, in part, through a grant from the Office of Fossil Energy, US Department of Energy (DE-FE-0009682). The authors acknowledge partial computational support through the Extreme Science and Engineering Discovery Environment (XSEDE). V.S. acknowledges the XSEDE computational resource allocation number TG-DMR160051.

■ REFERENCES

(1) Zhu, J.; Li, H.; Zhong, L.; Xiao, P.; Xu, X.; Yang, X.; Zhao, Z.; Li, J. Perovskite oxides: Preparation, Characterizations and applications in heterogeneous catalysis. *ACS Catal.* **2014**, *4*, 2917−2940.

(2) Voorhoeve, R. J. H.; Johnson, D. W.; Remeika, J. P.; Gallagher, P. K. Perovskite Oxides: Materials Science in Catalysis. *Science* **1977**, *195*, 827−833.

(3) Ran, R.; Wu, X.; Weng, D.; Fan, J. Oxygen storage capacity and structural properties of Ni-doped $LaMnO_3$ perovskites. *J. Alloys Compd.* **2013**, *577*, 288−294.

(4) Hébert, S.; Martin, C.; Maignan, A.; Retoux, R.; Hervieu, M.; Nguyen, N.; Raveau, B. Induced ferromagnetism in $LaMnO_3$ by Mn-site substitution: The major role of Mn mixed valency. *Phys. Rev. B: Condens. Matter Mater. Phys.* **2002**, *65*, 104420.

(5) Ghosh, K.; Ogale, S.; Ramesh, R.; Greene, R.; Venkatesan, T.; Gapchup, K.; Bathe, R.; Patil, S. Transition-element doping effects in $La_{0.7}Ca_{0.3}MnO_3$. *Phys. Rev. B: Condens. Matter Mater. Phys.* **1999**, *59*, 533−537.

(6) Jacobson, A. J. Materials for Solid Oxide Fuel Cells. *Chem. Mater.* **2010**, *22*, 660−674.

(7) Kuklja, M. M.; Kotomin, E. a.; Merkle, R.; Mastrikov, Y. a.; Maier, J. Combined theoretical and experimental analysis of processes determining cathode performance in solid oxide fuel cells. *Phys. Chem. Chem. Phys.* **2013**, *15*, 5443−5471.

(8) Mathur, N. D.; Burnell, G.; Isaac, S. P.; Jackson, T. J.; Teo, B.-S.; MacManus-Driscoll, J. L.; Cohen, L. F.; Evetts, J. E.; Blamire, M. G. Large low-field magnetoresistance in $La_{0.7}Ca_{0.3}MnO_3$ induced by artificial grain boundaries. *Nature* **1997**, *387*, 266−268.

(9) Giebeler, L.; Kießling, D.; Wendt, G. $LaMnO_3$ Perovskite Supported Noble Metal Catalysts for the Total Oxidation of Methane. *Chem. Eng. Technol.* **2007**, *30*, 889−894.

(10) Sharma, V.; Mahapatra, M. K.; Singh, P.; Ramprasad, R. Cationic surface segregation in doped $LaMnO_3$. *J. Mater. Sci.* **2015**, *50*, 3051−3056.

(11) Muñoz-García, A. B.; Ritzmann, A. M.; Pavone, M.; Keith, J. A.; Carter, E. A. Oxygen transport in perovskite-type solid oxide fuel cell materials: Insights from quantum mechanics. *Acc. Chem. Res.* **2014**, *47*, 3340−3348.

(12) Pavone, M.; Muñoz-García, A. B.; Ritzmann, A. M.; Carter, E. A. First-Principles Study of Lanthanum Strontium Manganite: Insights into Electronic Structure and Oxygen Vacancy Formation. *J. Phys. Chem. C* **2014**, *118*, 13346−13356.

(13) Lee, W.; Han, J. W.; Chen, Y.; Cai, Z.; Yildiz, B. Cation size mismatch and charge interactions drive dopant segregation at the surfaces of Manganite perovskites. *J. Am. Chem. Soc.* **2013**, *135*, 7909−25.

(14) Pavone, M.; Ritzmann, A. M.; Carter, E. a. Quantum-mechanics-based design principles for solid oxide fuel cell cathode materials. *Energy Environ. Sci.* **2011**, *4*, 4933.

(15) Lee, Y.-L.; Kleis, J.; Rossmeisl, J.; Shao-Horn, Y.; Morgan, D. Prediction of solid oxide fuel cell cathode activity with first-principles descriptors. *Energy Environ. Sci.* **2011**, *4*, 3966.

(16) Sharma, V.; Mahapatra, M. K.; Krishnan, S.; Thatcher, Z.; Huey, B. D.; Singh, P.; Ramprasad, R. Effects of Moisture on (La, A)MnO_3 (A = Ca, Sr, Ba) Solid Oxide Fuel Cell Cathodes: A First-principles and Experimental Study. *J. Mater. Chem. A* **2016**, *4*, 5605−5615.

(17) Pilania, G.; Mannodi-Kanakkithodi, A.; Uberuaga, B. P.; Ramprasad, R.; Gubernatis, J. E.; Lookman, T. Machine learning bandgaps of double perovskites. *Sci. Rep.* **2016**, *6*, 19375.

(18) Botu, V.; Mhadeshwar, A. B.; Suib, S. L.; Ramprasad, R. In *Information Science for Materials Discovery and Design*; Lookman, T., Alexander, F. J., Rajan, K., Eds.; Springer Series in Materials Science; Springer International Publishing: Cham, 2016; Vol. *225*; pp 157−172.

(19) Sharma, V.; Wang, C.; Lorenzini, R. G.; Ma, R.; Zhu, Q.; Sinkovits, D. W.; Pilania, G.; Oganov, A. R.; Kumar, S.; Sotzing, G. A.; et al. Rational design of all organic polymer dielectrics. *Nat. Commun.* **2014**, *5*, 4845.

(20) Meredig, B.; Wolverton, C. Dissolving the Periodic Table in Cubic Zirconia: Data Mining to Discover Chemical Trends. *Chem. Mater.* **2014**, *26*, 1985−1991.

(21) Castelli, I. E.; Jacobsen, K. W. Designing rules and probabilistic weighting for fast materials discovery in the Perovskite structure. *Modell. Simul. Mater. Sci. Eng.* **2014**, *22*, 055007.

(22) Curtarolo, S.; Hart, G. L. W.; Nardelli, M. B.; Mingo, N.; Sanvito, S.; Levy, O. The high-throughput highway to computational materials design. *Nat. Mater.* **2013**, *12*, 191−201.

(23) Sharma, V.; Pilania, G.; Rossetti, G. A.; Slenes, K.; Ramprasad, R. Comprehensive examination of dopants and defects in $BaTiO_3$ from first principles. *Phys. Rev. B: Condens. Matter Mater. Phys.* **2013**, *87*, 134109.

(24) D'Avezac, M.; Luo, J.-W.; Chanier, T.; Zunger, A. Genetic-Algorithm Discovery of a Direct-Gap and Optically Allowed Superstructure from Indirect-Gap Si and Ge Semiconductors. *Phys. Rev. Lett.* **2012**, *108*, 027401.

DOI: 10.1021/acs.jpcc.6b04524
J. Phys. Chem. C 2016, 120, 22126−22133

(25) Lin, L.-C.; Berger, A. H.; Martin, R. L.; Kim, J.; Swisher, J. A.; Jariwala, K.; Rycroft, C. H.; Bhown, A. S.; Deem, M. W.; Haranczyk, M.; et al. In silico screening of carbon-capture materials. *Nat. Mater.* **2012**, *11*, 633−641.
(26) Hachmann, J.; Olivares-Amaya, R.; Atahan-Evrenk, S.; Amador-Bedolla, C.; Sanchez-Carrera, R. S.; Gold-Parker, A.; Vogt, L.; Brockway, A. M.; Aspuru-Guzik, A. The Harvard Clean Energy Project: Large-Scale Computational Screening and Design of Organic Photovoltaics on the World Community Grid. *J. Phys. Chem. Lett.* **2011**, *2*, 2241−2251.
(27) Jain, A.; Hautier, G.; Moore, C. J.; Ping Ong, S.; Fischer, C. C.; Mueller, T.; Persson, K. A.; Ceder, G. A high-throughput infrastructure for density functional theory calculations. *Comput. Mater. Sci.* **2011**, *50*, 2295−2310.
(28) Greeley, J.; Jaramillo, T. F.; Bonde, J.; Chorkendorff, I.; Nørskov, J. K. Computational high-throughput screening of electro-catalytic materials for hydrogen evolution. *Nat. Mater.* **2006**, *5*, 909−913.
(29) Ceder, G.; Chiang, Y.-M.; Sadoway, D. R.; Aydinol, M. K.; Jang, Y.-I.; Huang, B. Identification of cathode materials for lithium batteries guided by first principles calculations. *Nature* **1998**, *392*, 694−696.
(30) Mannodi-Kanakkithodi, A.; Pilania, G.; Huan, T. D.; Lookman, T.; Ramprasad, R. Machine Learning Strategy for Accelerated Design of Polymer Dielectrics. *Sci. Rep.* **2016**, *6*, 20952.
(31) Ma, R.; Sharma, V.; Baldwin, A. F.; Tefferi, M.; Offenbach, I.; Cakmak, M.; Cao, Y.; Ramprasad, R.; Sotzing, G. A. Rational Design and Synthesis of Polythioureas as Capacitor Dielectrics. *J. Mater. Chem. A* **2015**, *3*, 14845.
(32) Baldwin, A. F.; Ma, R.; Mannodi-Kanakkithodi, A.; Huan, T. D.; Wang, C.; Tefferi, M.; Marszalek, J. E.; Cakmak, M.; Cao, Y.; Ramprasad, R.; et al. Poly(dimethyltin glutarate) as a prospective material for high dielectric applications. *Adv. Mater.* **2015**, *27*, 346−351.
(33) Gautier, R.; Zhang, X.; Hu, L.; Yu, L.; Lin, Y.; Sunde, T. O. L.; Chon, D.; Poeppelmeier, K. R.; Zunger, A. Prediction and accelerated laboratory discovery of previously unknown 18-electron ABX compounds. *Nat. Chem.* **2015**, *7*, 308−316.
(34) Lorenzini, R. G.; Kline, W. M.; Wang, C. C.; Ramprasad, R.; Sotzing, G. A. The rational design of polyurea & polyurethane dielectric materials. *Polymer* **2013**, *54*, 3529−3533.
(35) Peng, H.; Zakutayev, A.; Lany, S.; Paudel, T. R.; D'Avezac, M.; Ndione, P. F.; Perkins, J. D.; Ginley, D. S.; Nagaraja, A. R.; Perry, N. H.; et al. Li-doped Cr_2MnO_4: A new p-type transparent conducting oxide by computational materials design. *Adv. Funct. Mater.* **2013**, *23*, 5267−5276.
(36) Nørskov, J. K.; Bligaard, T.; Rossmeisl, J.; Christensen, C. H. Towards the computational design of solid catalysts. *Nat. Chem.* **2009**, *1*, 37−46.
(37) Balke, B.; Wurmehl, S.; Fecher, G. H.; Felser, C.; Kubler, J. Rational design of new materials for spintronics: Co_2FeZ (Z = Al, Ga, Si, Ge). *Sci. Technol. Adv. Mater.* **2008**, *9*, 014102.
(38) Mueller, T.; Kusne, A. G.; Ramprasad, R.; Parill, A. L.; Lipkowitz, K. B. *Rev. Comput. Chem.* **2016**, *29*, 186.
(39) Norby, P.; Andersen, I.; Andersen, E.; Andersen, N. The crystal structure of lanthanum manganate(III), $LaMnO_3$, at room temperature and at 1273 K under N2. *J. Solid State Chem.* **1995**, *119*, 191−196.
(40) Kresse, G.; Furthmüller, J. Efficiency of ab-initio total energy calculations for metals and semiconductors using a plane-wave basis set. *Comput. Mater. Sci.* **1996**, *6*, 15−50.
(41) Kresse, G.; Furthmüller, J. Efficient iterative schemes for ab initio total-energy calculations using a plane-wave basis set. *Phys. Rev. B: Condens. Matter Mater. Phys.* **1996**, *54*, 11169−11186.
(42) Perdew, J. P.; Burke, K.; Ernzerhof, M. Generalized Gradient Approximation Made Simple. *Phys. Rev. Lett.* **1996**, *77*, 3865−3868.
(43) Blöchl, P. E. Projector augmented-wave method. *Phys. Rev. B: Condens. Matter Mater. Phys.* **1994**, *50*, 17953−17979.
(44) Castelli, I. E.; Landis, D. D.; Thygesen, K. S.; Dahl, S.; Chorkendorff, I.; Jaramillo, T. F.; Jacobsen, K. W. New cubic perovskites for one- and two-photon water splitting using the computational materials repository. *Energy Environ. Sci.* **2012**, *5*, 9034−9043.
(45) Akbarzadeh, A. R.; Ozolinš, V.; Wolverton, C. First-Principles Determination of Multicomponent Hydride Phase Diagrams: Application to the Li-Mg-N-H System. *Adv. Mater.* **2007**, *19*, 3233−3239.
(46) Akbarzadeh, A. R.; Wolverton, C.; Ozolins, V. First-principles determination of crystal structures, phase stability, and reaction thermodynamics in the Li-Mg-Al-H hydrogen storage system. *Phys. Rev. B: Condens. Matter Mater. Phys.* **2009**, *79*, 184102.
(47) Nicholson, K. M.; Chandrasekhar, N.; Sholl, D. S. Powered by DFT: Screening Methods That Accelerate Materials Development for Hydrogen in Metals Applications. *Acc. Chem. Res.* **2014**, *47*, 3275−3283.
(48) Duan, Y.; Zhang, B.; Sorescu, D. C.; Johnson, J. K. CO2 capture properties of MCOH (M = Li, Na, K) systems: A combined density functional theory and lattice phonon dynamics study. *J. Solid State Chem.* **2011**, *184*, 304−311.
(49) KHAZANA: A Computational Materials Knowledgebase. http://khazana.uconn.edu/.
(50) Wang, L.; Maxisch, T.; Ceder, G. Oxidation energies of transition metal oxides within the GGA + U framework. *Phys. Rev. B: Condens. Matter Mater. Phys.* **2006**, *73*, 195107.
(51) Lee, Y.-L.; Kleis, J.; Rossmeisl, J.; Morgan, D. Ab initio energetics of $LaBO_3$(001) (B = Mn, Fe, Co, and Ni) for solid oxide fuel cell cathodes. *Phys. Rev. B: Condens. Matter Mater. Phys.* **2009**, *80*, 224101.
(52) Anisimov, V. I.; Aryasetiawan, F.; Lichtenstein, A. I. First-principles calculations of the electronic structure and spectra of strongly correlated systems: the LDA + U method. *J. Phys.: Condens. Matter* **1997**, *9*, 767−808.
(53) Franchini, C.; Podloucky, R.; Paier, J.; Marsman, M.; Kresse, G. Ground-state properties of multivalent manganese oxides: Density functional and hybrid density functional calculations. *Phys. Rev. B: Condens. Matter Mater. Phys.* **2007**, *75*, 195128.
(54) Das, S.; Dey, T. K. Magnetocaloric effect in potassium doped lanthanum Manganite perovskites prepared by a pyrophoric method. *J. Phys.: Condens. Matter* **2006**, *18*, 7629−7641.
(55) Rørmark, L.; Stølen, S.; Wiik, K.; Grande, T. Enthalpies of Formation of $La_{1x}A_xMnO_3\delta$ (A = Ca and Sr) Measured by High-Temperature Solution Calorimetry. *J. Solid State Chem.* **2002**, *163*, 186−193.
(56) Jacob, K. T.; Attaluri, M. Refinement of thermodynamic data for $LaMnO_3$. *J. Mater. Chem.* **2003**, *13*, 934−942.
(57) Nikam, S. K.; Athawale, A. A. Phase formation study of noble metal (Au, Ag and Pd) doped lanthanum perovskites synthesized by hydrothermal method. *Mater. Chem. Phys.* **2015**, *155*, 104−112.
(58) Ning, Z.; Tao, G.; Hong-Xia, C.; Jian-Chun, B. Chemical composition and magnetism of Ag doped $LaMnO_3$. *Chin. Phys. B* **2008**, *17*, 317−322.
(59) Narsinga Rao, G.; Roy, S.; Yang, R. C.; Chen, J. W. Double peak behavior of resistivity curves in Cd doped $LaMnO_3$ perovskite systems. *J. Magn. Magn. Mater.* **2003**, *260*, 375−379.
(60) Gao, T.; Cao, S.; Liu, Y.; Zhang, Y.; Zhang, J. Cu-doping induced ferromagnetic insulating behavior and domain wall pinning effects in $LaMnO_3$. *Rare Met.* **2011**, *30*, 359−367.
(61) Hastie, T.; Tibshirani, R.; Friedman, J. *The Elements of Statistical Learning: Data Mining, Inference, and Prediction*, 2nd ed.; Springer: New York; 2009.
(62) Muller, K.-R.; Mika, S.; Ratsch, G.; Tsuda, K.; Scholkopf, B. An introduction to kernel-based learning algorithms. *IEEE Trans. Neural Networks* **2001**, *12*, 181−201.
(63) Hofmann, T.; Schölkopf, B.; Smola, A. J. Kernel methods in machine learning. *Ann. Stat.* **2008**, *36*, 1171−1220.
(64) Albanese, D.; Visintainer, R.; Merler, S.; Riccadonna, S.; Jurman, G.; Furlanello, C. mlpy: Machine learning Python. *arXiv Prepr.* **2012**, 1202.6548.

DOI: 10.1021/acs.jpcc.6b04524
J. Phys. Chem. C 2016, 120, 22126−22133

(65) Rupp, M.; Tkatchenko, A.; Müller, K.-R.; von Lilienfeld, O. A. Fast and Accurate Modeling of Molecular Atomization Energies with Machine Learning. *Phys. Rev. Lett.* **2012**, *108*, 058301.
(66) Botu, V.; Ramprasad, R. Adaptive machine learning framework to accelerate ab initio molecular dynamics. *Int. J. Quantum Chem.* **2015**, *115*, 1074−1083.
(67) Ramakrishnan, R.; von Lilienfeld, O. A. Many Molecular Properties from One Kernel in Chemical Space. *Chimia* **2015**, *69*, 182−186.
(68) Huan, T. D.; Mannodi-Kanakkithodi, A.; Ramprasad, R. Accelerated materials property predictions and design using motif-based fingerprints. *Phys. Rev. B: Condens. Matter Mater. Phys.* **2015**, *92*, 014106.
(69) Shannon, R. D. Revised effective ionic radii and systematic studies of interatomic distances in halides and chalcogenides. *Acta Crystallogr., Sect. A: Cryst. Phys., Diffr., Theor. Gen. Crystallogr.* **1976**, *32*, 751−767.

DOI: 10.1021/acs.jpcc.6b04524
J. Phys. Chem. C 2016, 120, 22126−22133